HENLE FIBER LAYER THICKNESS AND AREA MEASUREMENT IN TYPE 2 DIABETES MELLITUS WITH AND WITHOUT RETINOPATHY USING A MODIFIED DIRECTIONAL OPTICAL COHERENCE TOMOGRAPHY STRATEGY

M. GIRAY ERSOZ, MD,* FURKAN KIRIK, MD,† BURCU ISIK, MD,* HAKAN OZDEMIR, MD†

Purpose: To investigate the thicknesses and areas of Henle fiber layer (HFL), outer nuclear layer, and outer plexiform layer in the eyes of patients with diabetes with no diabetic retinopathy, in eyes with nonproliferative diabetic retinopathy without diabetic macular edema, and in healthy eyes using a modified directional optical coherence tomography strategy.

Methods: In this prospective study, the no diabetic retinopathy group included 79 participants, the nonproliferative diabetic retinopathy group comprised 68 participants, and the control group had 58 participants. Thicknesses and areas of Henle fiber layer, outer nuclear layer, and outer plexiform layer were measured on a horizontal single optical coherence tomography scan centered on the fovea using directional optical coherence tomography.

Results: The foveal, parafoveal, and total HFL were significantly thinner in the nonproliferative diabetic retinopathy group than in the no diabetic retinopathy group and the control group (all $P < 0.05$). The no diabetic retinopathy group had significantly thinner foveal HFL thickness and area compared with the control group (all $P < 0.05$). The nonproliferative diabetic retinopathy group had significantly thicker outer nuclear layer thickness and area in all regions than the other groups (all $P < 0.05$). The outer plexiform layer measurements did not differ between the groups (all $P > 0.05$).

Conclusion: Directional optical coherence tomography provides isolated thickness and area measurement of HFL. In patients with diabetes, the HFL is thinner, and HFL thinning begins before the presence of diabetic retinopathy.

RETINA 43:1097–1106, 2023

Diabetic retinopathy (DR) is the leading cause of vision loss and blindness in patients aged 20 years to 74 years.[1] Diabetic retinopathy is a retinal microvascular and neurodegenerative complication of diabetes mellitus (DM).[2] In early DR, optical coherence tomography (OCT) showed a decrease in inner retinal layer thickness, an increase in the inner nuclear layer/outer plexiform layer complex, and no changes in the outer nuclear layer (ONL). The increased thickness of inner nuclear layer/outer plexiform layer complex was attributed to hypertrophy of Müller cell nuclei, which are located in the INL.[3,4]

Henle fiber layer (HFL), composed of the axons of photoreceptors and the outer processes of the Z-shaped Müller cells, is located between the outer plexiform layer (OPL) and ONL in the macula.[4–7] Henle fiber layer appears hyporeflective and cannot be distinguished from ONL on an untilted OCT scan. If the pupil entry position of the OCT beam is changed temporally or nasally and a tilted OCT scan is obtained (directional OCT), HFL appears hyperreflective at the contrary site and cannot be distinguished from OPL.[8,9] Therefore, HFL influences thickness measurements of both the ONL and the OPL, especially ONL. Henle

fiber layer also has importance in diabetic macular edema pathophysiology. Deeply located microaneurysms directly leak into the HFL.[10] Moreover, cystoid spaces start to form in the HFL.[5]

In this study, we aimed to investigate the thicknesses of HFL, ONL, and OPL in the eyes of patients with diabetes with no DR (NDR), eyes with nonproliferative diabetic retinopathy (NPDR) without diabetic macular edema, and in healthy eyes using directional OCT. We also compared the thicknesses of these retinal layers between different stages of nonproliferative DR.

Methods

This prospective study was conducted between October 2021 and March 2022 after ethics committee approval had been obtained. Written informed consent was obtained from all participants. The study adhered to the tenets of the Declaration of Helsinki. Patients with Type 2 DM were divided into NDR or NPDR (without diabetic macular edema) groups. Each group was matched for age, sex, and refractive index. For each subject, the eye with the highest OCT image quality score was selected for analysis. Eyes with NPDR were stratified into three groups (mild, moderate, and severe) according to the International Clinical Diabetic Retinopathy and Diabetic Macular Edema Disease Severity Scales.[11]

All subjects underwent ophthalmic examinations, including best-corrected visual acuity, anterior segment and dilated posterior segment examination, and SD-OCT scanning (Spectralis OCT; Heidelberg Engineering, Heidelberg, Germany).

Exclusion Criteria

Subjects with a history of ocular surgery, ocular diseases such as uveitis, glaucoma, retinal disorders (other than DR for the NPDR group), and optic nerve abnormalities were excluded. Subjects with spherical equivalent refractive errors between −3.0 and +3.0 diopters were included in the study. Patients with DM duration of <5 years were excluded from NDR and NPDR groups. Eyes with clinically significant diabetic macular edema, any cystoid space detected on 20° × 20° macular OCT scans, and a history of intravitreal anti–vascular endothelial growth factor injection, intravitreal dexamethasone implantation, or retinal argon laser photocoagulation were also excluded from the NPDR group. Eyes with small hard exudates that could not be detected in posterior segment examination and could only be seen as the hyperreflective dot on OCT were not excluded. All eyes were evaluated by the same experienced retinal specialist (H.O.) for exclusion criteria and severity of DR.

Image Acquisition and Henle Fiber Layer, Outer Plexiform Layer, and Outer Nuclear layer Thickness and Area Measurements

First, the C-curve (mean keratometry values) and refractive error of each participant were incorporated into Spectralis SD-OCT scan acquisition. In contrast to previous studies,[8,9] we did not use axial length to correct retinal magnification because the Spectralis software estimates the axial length based on the total refraction of the eye and the C-curve entered in the software. Based on the C-curve, the software then uses this information to incorporate retinal magnification, and with that, an estimate of the intraocular lateral pixel scaling is done.[12,13]

The fovea was evaluated using a single 30° horizontal SD-OCT scan, with an average of 100 images in a centered direction (central pupil entry position). This first image was set as a reference. Although the subject remained at the chin rest, the same foveal 30° horizontal line was scanned using follow-up mode with an average of 100 images in a decentered direction by lifting the temporal and then nasal side of the image (temporal and nasal pupil entry position, respectively) as previously described and two additional tilted OCT images were obtained.[8,9,14] To obtain these oblique images, we moved the joystick of the device 1.5 mm to 2 mm from the middle position, where we took the first image, toward the nasal and temporal directions, with the help of a ruler. Henle fiber layer appeared hyperreflective at the nasal side and more hyporeflective than the ONL at the temporal side on tilted OCT images with a temporal pupil entry position and vice versa (Figure 1).

For the HFL thickness and area measurements, each retinal layer was measured on these two tilted images using built-in automated segmentation software (Segmentation Technology; Heidelberg Engineering). The

From the *Department of Ophthalmology, Biruni University Medical School, Istanbul, Turkey; and †Department of Ophthalmology, Faculty of Medicine, Bezmialem Vakif University, Istanbul, Turkey.

The manuscript has not been presented at any congress or evaluated in any form by another journal.

None of the authors has any financial/conflicting interests to disclose.

The authors had full access to all the data in the study and take full responsibility for the integrity and the accuracy of the data, as well as the decision to submit it for publication. All authors approved the manuscript and its submission.

Reprint requests: Hakan Ozdemir, MD, Department of Ophthalmology, Faculty of Medicine, Bezmialem Vakif University, Adnan Menderes, Bulvarı (Vatan Cad.) Fatih, Istanbul 34093, Turkey; e-mail: hozdemir72@hotmail.com

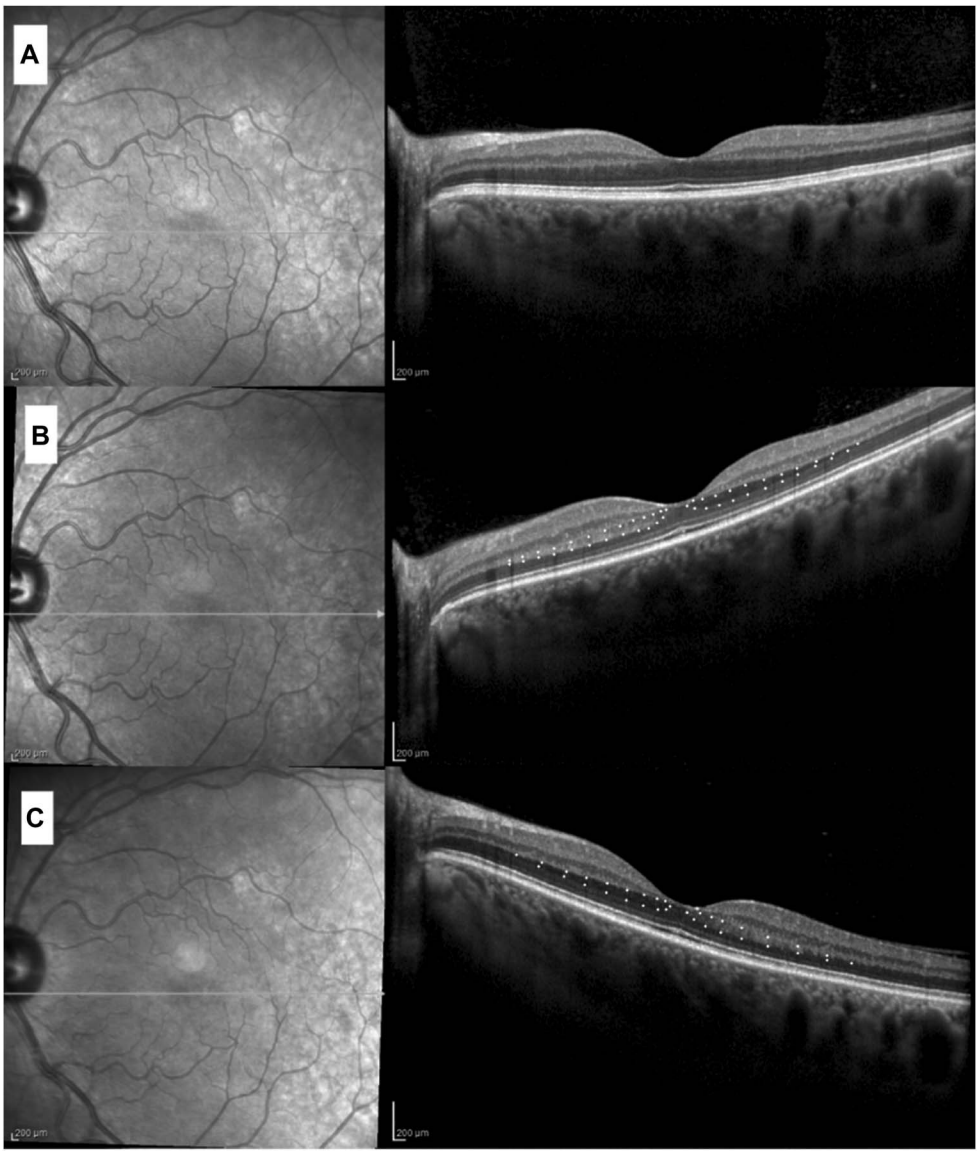

Fig. 1. Horizontal cross-sectional OCT scans of a 48-year-old healthy man were obtained by directing the laser beam to the retina of the left eye at different orientations. Henle fiber layer, whose visibility varies as a result of decentered laser beams directed toward the retina from the nasal and temporal entry positions of the pupil, is indicated with white dots. **A.** In this pupil-centered and nontilted OCT scan, the HFL under the OPL cannot be clearly visualized because it has isoreflectivity with the ONL. The directional (**B**) and (**C**) scans were performed in the "follow-up" mode after being centered; (**A**) scan was set as the reference image. **B.** In directional OCT performed from the temporal entry position of the pupil, a temporal-upward retinal scan was obtained. Because of the oblique orientation of Müller cells and photoreceptor axons, the HFL acquires hyperreflectivity similar to the OPL in the nasal hemiretina, whereas it appears hyporeflective in the temporal hemiretina. **C.** Nasally decentered directional OCT scanning was also performed with the nasal pupil entry position of the laser beam. In contrast to the image (**B**), HFL appears hyporeflective on the nasal side and hyperreflective on the temporal side.

software considered hyperreflective HFL in OPL and hyporeflective HFL in ONL. Then, one of these tilted images was set as a reference, and the OPL thicknesses of these two tilted images were compared using the follow-up option of the software (Figure 2A, B). In the output graph of this comparison, OPL thickness differences between these two tilted images appeared as red and green areas. These red and green areas indicate the HFL (Figures 2, 3). At selected locations, the Spectralis software can automatically measure the HFL thickness as the OPL thickness differences between these two tilted images and display it as a value in parentheses (Figure 3). We measured HFL thicknesses at eight different points between 100 μm and 1,500 μm from the foveal center, with 200 μm intervals, on both the temporal and the nasal sides (total of 16 points). For the HFL area measurement, the image of the "OPL thickness profile" graph (scale range 0.5 mm; Figure 2B) indicating the thickness differences was exported as a .jpg file. Then the image was imported into ImageJ/Fiji (http://fiji.sc./Fiji). First, the pixel-to-aspect ratio was calculated based on the pixel equivalent of the micron length on the horizontal and vertical axes of the graph, and the image was scaled (set scale function) by selecting the 500 μm horizontal line. The polygon tool was then used for the manual selection of the region of interest, and all HFL areas horizontally at 500 μm and 1,500 μm distances from the foveal center at both temporal and nasal sides were manually selected. Each region of interest was measured using the analyze–measure option, and total (horizontally 3,000 μm, centered fovea), foveal (horizontally 1,000 μm,

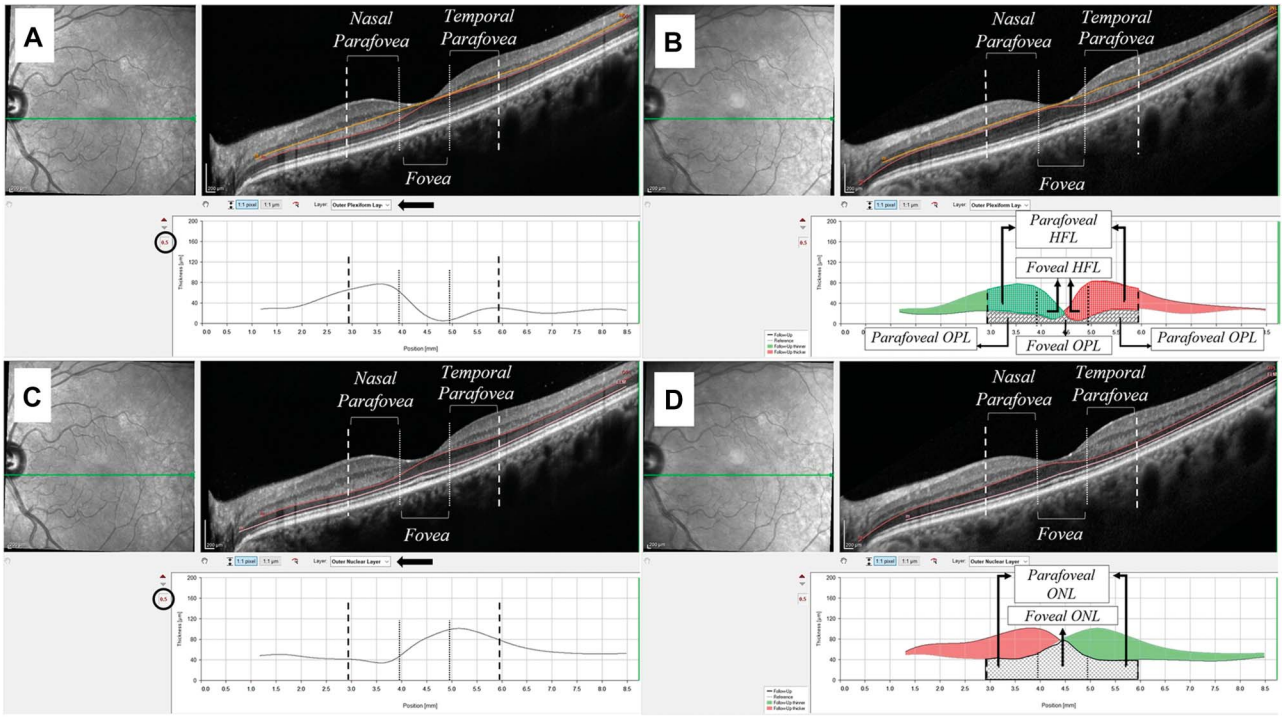

Fig. 2. Area measurement of HFL, ONL, and OPL using directional OCT in the left eye of a 48-year-old healthy man. After the temporally decentered OCT scan (**A** and **C**) was set as the reference image and the nasally decentered OCT scan (**B** and **D**) as the follow-up image using the follow-up option, "thickness profile" graphs of OPL (**B**) and ONL (**D**) that showed positional thickness differences between nasally decentered and temporally decentered OCT images were obtained. **A** and **C.** The selection of the retinal layer was to be evaluated as indicated by the black arrow, and the vertical scale range of the graphs was set to 0.5 mm (black circle). The area under the black line in the graphs shows the thickness distribution of the retinal layer evaluated. Temporally decentered OCT scan shows a thicker OPL and thinner ONL because of the hyperreflectivity of the HFL in the nasal hemiretina, whereas a contrasting thickness distribution to the nasal is observed in the temporal hemiretina. **B** and **D.** In the thickness profile graph of the nasally decentered OCT scan, the thickness change is calculated automatically according to the reference (temporally decentered) image. The green-filled area indicates reduced thickness, and the red-filled region indicates retinal locations with increased thickness. Because only the visibility of the HFL changes according to the OCT direction, the red and green areas indicate the HFL. The unfilled regions of graphs below the black line are the HFL removed OPL (**B**) or ONL area (**D**). The HFL, OPL, and ONL areas in the foveal and parafoveal regions were measured manually with the assistance of ImageJ polygonal selection (pixel-to-aspect ratio adjusted). Henle fiber layer area measurement was performed on the OPL thickness profile graph (**B**).

centered fovea), and parafoveal (total minus foveal) HFL areas were obtained.

The white area under the green and red areas on the image of the "OPL thickness profile" graph indicates the HFL removed OPL. We measured the OPL area on this white area using the same steps as in HFL area measurements (Figure 2B). Outer plexiform layer thicknesses were measured at the same 16 locations used in the HFL thickness measurement. On the green side of the graph, "the current OPL thickness" indicates "HFL removed OPL thickness." On the red side of the graph, "the current value of OPL thickness" minus "the HFL thickness at this location" indicates "HFL removed OPL thickness" (Figure 3A, B).

For ONL thickness and area measurement, the "ONL thickness profile" graph (scale range 0.5 mm) of comparison between two tilted OCT images was used. The white area under the green and red areas on the image of the "ONL thickness profile" graph indicates the HFL removed ONL. The same steps for OPL area measurement were used to measure the ONL area (Figure 2D). Outer nuclear layer thicknesses were measured at the same 16 locations used in HFL and OPL thickness measurements. On the green side of the graph, "the current ONL thickness" indicates "HFL removed ONL thickness." On the red side of the graph, "the current value of ONL thickness" minus "the value in the parentheses (the HFL thickness at this location)" indicates "HFL removed ONL thickness" (Figure 3C, D).

Mean thicknesses measured at six foveal points (foveal thickness), 10 parafoveal points (parafoveal thickness), and all 16 points (total thickness) for each of HFL, OPL, and ONL were used for statistical analysis. In addition to the measurement of HFL, OPL, and ONL thicknesses in tilted scans, thickness measurement of ONL in nontilted, centered scan (c-ONL) without excluding HFL (from the lower border of the OPL to the external limiting membrane) was performed from the same points.

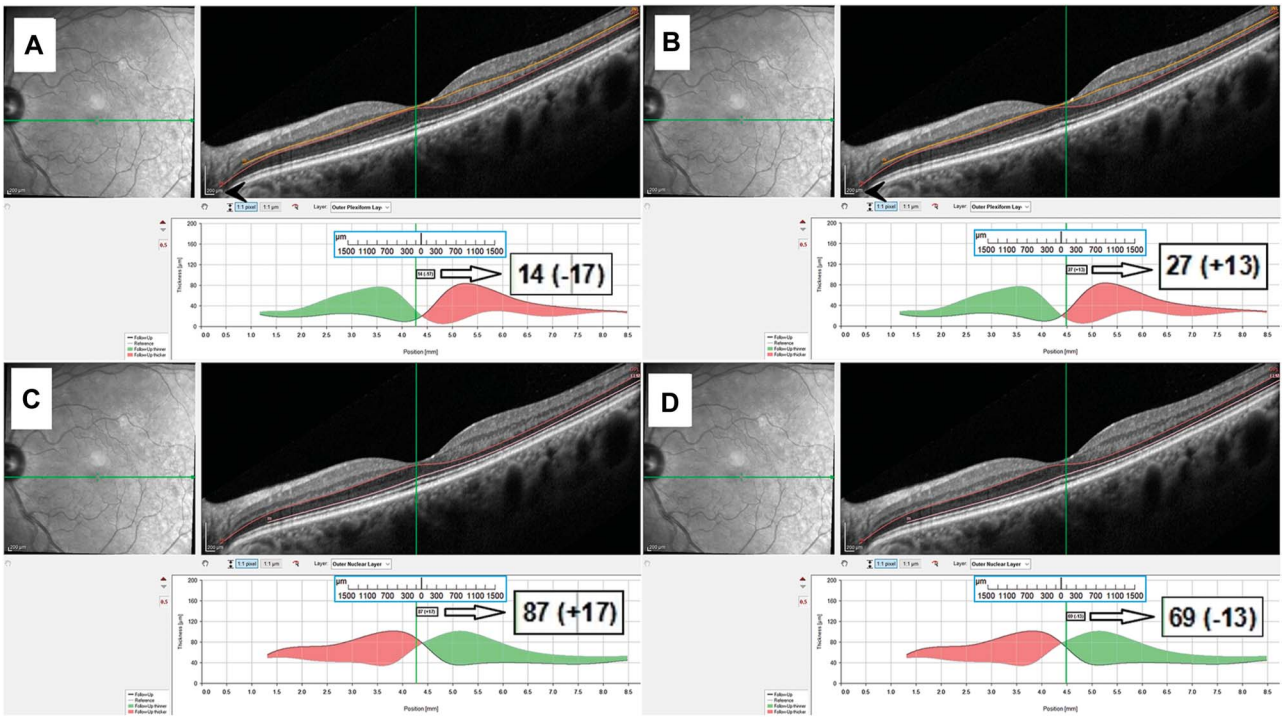

Fig. 3. Thickness measurements of HFL, ONL, and OPL in the left eye of a 48-year-old healthy man (same participant as in Figure 2) performed 100 μm (**A** and **C** nasal; **B** and **D** temporal) away from the fovea using directional OCT. After the temporally decentered OCT scan (shown in Figure 2) was set as the reference image and the nasally decentered OCT scan (**A**–**D**) as the follow-up image using the follow-up option, "thickness profile" graphs of OPL (**A** and **B**) and ONL (**C** and **D**) that showed positional thickness differences between nasally decentered and temporally decentered OCT images were obtained. **A**–**D.** The green position marker integrated into the OCT device was used for thickness measurements. Locations for thickness measurement were determined with an eye-specific external ruler (presented with a blue boundary) formed in accordance with the horizontal 200-μm dimension of the scale (black arrowheads). In both the red and the green regions of the OPL and ONL thickness profile graph, the HFL thickness at the selected point is indicated in parentheses. **A.** On the green region of the OPL thickness profile graph, "the current OPL thickness" indicates "HFL removed OPL thickness." **B.** On the red region of this graph, "the current OPL thickness" minus "the HFL thickness at this location" indicates "HFL removed OPL thickness." **C** and **D.** After the OPL and HFL thicknesses were recorded, the ONL thickness measurement at the selected location was recorded by switching to the ONL thickness profile graph, keeping the position marker at the same location. **C.** On the red side of the graph, "the current value of ONL thickness" minus "the value in the parenthesis (the HFL thickness at this location)" indicates "HFL removed ONL thickness." **D.** On the green side of this graph, "the current ONL thickness" indicates "HFL removed ONL thickness."

All OCT scans of all participants were obtained by the same technician. All thickness and area measurements analyzed to compare the NPDR, NDR, and control group were performed by another investigator (F.K.) masked to the label of participants. Before measurements, OPL and ONL segmentations were checked by the same investigator in all scans, and incorrect auto-segmentations were manually corrected (Figure 4). Sixteen randomly selected participants of the control group were analyzed for intervisit, interobserver, and intraobserver agreements. To investigate intervisit reproducibility, the subject was instructed to take a 5-minute break outside the machine to reset the OCT. After this interval, the OCT scanning protocol was repeated by the same technician, and measurements were also repeated by the same investigator (F.K.). To investigate interobserver and intraobserver agreements, the first OCT scans were used. The measurements were repeated by F.K. to investigate intraobserver agreement. Measurements of another investigator (M.G.E.) were compared with the first measurements of F.K. to analyze the interobserver agreement. Each observer manually corrected all segmentation errors by checking the INL (upper border of OPL), OPL (the boundary between OPL and ONL), and external limiting membrane (lower border of ONL) segmentation lines (Figure 4).

Central Macular Thickness Measurement

The 20° × 20° macular volumetric scanning protocol of the SD-OCT was performed for all participants, and the mean retinal thickness, which was automatically measured in the 1-mm-diameter fovea-centered region (central ring in the ETDRS grid), was recorded as the central macular thickness.

Statistical Analyses

Statistical analyses were performed using the SPSS version 22 software package (Chicago, IL). For

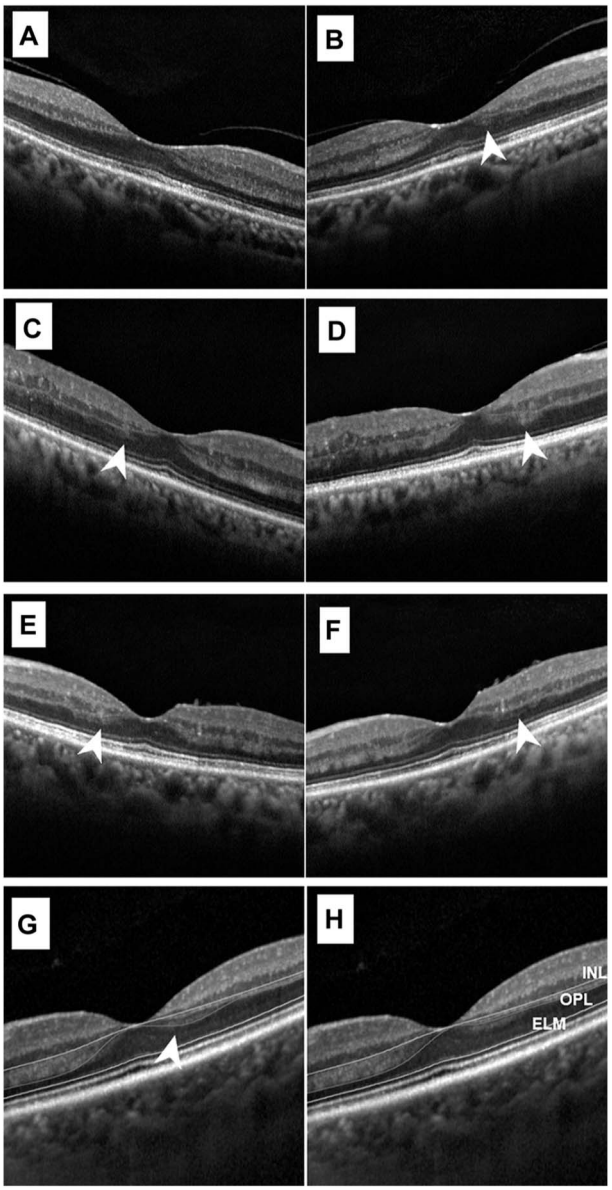

Fig. 4. Directional OCT scans showing localized hyperreflective alterations on the hyporeflective side of the HFL (white arrowheads) in eyes with nonproliferative diabetic retinopathy without macular edema (NPDR). **A** and **B.** A 51-year-old male patient with mild NPDR in the right eye. **B.** Hyperreflective HFL alteration appears in the temporal foveal area on a nasally decentered OCT scan. **C–F.** Directional OCT scans of 47- and 62-year-old female patients with severe NPDR (**C–E**). Hyperreflective HFL alterations are seen in both temporally (**C** and **F**) and nasally (**D** and **E**) decentered scans. **G** and **H.** Incorrect automated segmentations caused by conditions such as hyperreflective alteration in the HFL were corrected manually. **G.** Localized hyperreflectivity on the hyporeflective side of the HFL (white arrowhead) causes an incorrectly thicker auto-segmentation of the OPL. **H.** Incorrect segmentation was corrected manually by following the lower border of the OPL hyperreflectivity. In addition to the OPL segmentation line, the inner nuclear layer (INL) and external limiting membrane (ELM) segmentation lines were also checked.

comparisons of the groups, the Kruskal–Wallis test and the one-way analysis of variance were used for continuous variables, and Pearson chi-square test was used for categorical data. Intervisit, interobserver, and intraobserver agreements were investigated using the coefficient of variation and intraclass correlation coefficient with a two-way mixed and absolute agreement model. $P < 0.05$ was considered statistically significant.

Results

The NDR group included 79 participants, the NPDR group comprised 68 participants, and the control group had 58 participants. There was no significant difference between the groups regarding age, sex, axial length, and refractive error (Table 1). The OPL thicknesses, areas, and central macular thickness did not differ between the groups. The foveal, parafoveal, and total HFL areas and HFL thicknesses were significantly lower in the NPDR group than in the NDR group and control group (all $P < 0.05$). There were no significant differences between the NDR and control groups regarding parafoveal and total HFL thickness and area. However, the NDR group had significantly lower foveal HFL thickness and area compared with the control group ($P = 0.007$ and $P = 0.01$, respectively). In contrast to HFL thickness, the NPDR group had significantly higher ONL thickness and area in all regions than the other groups (all $P < 0.05$). There were no significant differences between the NDR and control groups regarding ONL thickness and area (Tables 1 and 2). There was no significant difference between the groups regarding the mean c-ONL thicknesses measured from nontilted scans (Table 2).

In 12 of 13 eyes (92.3%) in the severe NPDR group, 13 of 23 eyes (56.5%) in the moderate NPDR group, and 3 of 32 eyes (9.4%) in the mild NPDR group, localized hyperreflective areas were seen in the hyporeflective side of the HFL. There was no hyperreflective or hyporeflective HFL alteration in this hyperreflective area when the OCT beam was decentered in the opposite direction. There were no shadowing artifacts under any of these areas (Figure 4). We did not observe such a change in the NDR group or the control group.

The mild NPDR group comprised 32 eyes, the moderate NPDR group had 23 eyes, and the severe NPDR group constituted 13 eyes. These groups also had no differences regarding age, sex, duration of diabetes, HbA1c, refractive error, axial length, central macular thickness, OPL thickness, and area (Tables 3 and 4). The parafoveal HFL thickness and area did not differ between the NPDR groups. The foveal HFL thickness was lower in the severe NPDR group than in the other groups (all $P < 0.05$). The

Table 1. Comparisons of Demographic and Ocular Data and Area Measurements Between NDR, NPDR, and Control Groups

	Control (n = 58)	NDR (n = 79)	NPDR (n = 68)	*P*
Sex (male %)	29.3	35.4	45.6	0.2*
Age (years)	57.3 ± 7.9	56.8 ± 7.3	57.9 ± 7.2	0.7†
Refractive error (diopter)	1.2 ± 0.7	0.9 ± 0.9	1.1 ± 1.0	0.1†
Axial length (mm)	22.44 ± 0.8	22.52 ± 1.1	22.42 ± 0.9	0.6†
OPL area parafovea (μm^2)	34,224.8 ± 4,319.3	35,241.7 ± 4,821.6	35,946.6 ± 5,271.1	0.1†
OPL area fovea (μm^2)	9,790.5 ± 2,652.1	8,874 ± 2,396.8	9,161.8 ± 2,261.8	0.1†
OPL area total (μm^2)	44,015.4 ± 5,997.7	44,115.7 ± 5,942.8	45,108.4 ± 6,537.4	0.5†
HFL area parafovea (μm^2)	77,671.3 ± 9,378.7	78,236.2 ± 8,740.9	71,886.6 ± 9,688.2	<0.001‡
HFL area fovea (μm^2)	26,998.1 ± 4,737.9	24,490.3 ± 4,822.5	20,857.6 ± 5,382.7	<0.001‡
HFL area total (μm^2)	104,669.4 ± 11,546.1	102,726.5 ± 10,515.7	92,744.2 ± 11,872.0	<0.001‡
ONL area parafovea (μm^2)	61,863.7 ± 8,730	62,970.1± 9,016.5	72,081.1 ± 12,223.3	<0.001‡
ONL area fovea (μm^2)	60,889.2 ± 9,832.5	62,345.2 ± 9,322	69,063.8 ± 11,390	<0.001‡
ONL area total (μm^2)	122,753 ± 17,143.4	125,315.3 ± 16,259.4	141,144 ± 21,132.5	<0.001‡

Tukey HSD post hoc test for HFL-parafovea: control versus NDR, $P = 0.9$; control versus NPDR, $P = 0.002$; NDR versus NPDR, $P < 0.001$. Tukey HSD post hoc test for HFL-fovea: control versus NDR, $P = 0.01$; control versus NPDR, $P < 0.001$; NDR versus NPDR, $P < 0.001$. Tukey HSD post hoc test for HFL-total: control versus NDR, $P = 0.6$; control versus NPDR, $P < 0.001$; NDR versus NPDR, $P < 0.001$. Tukey HSD post hoc test for ONL-parafovea: control versus NDR, $P = 0.8$; control versus NPDR, $P < 0.001$; NDR versus NPDR, $P < 0.001$. Tukey HSD post hoc test for ONL-fovea: control versus NDR, $P = 0.7$; control versus NPDR, $P < 0.001$; NDR versus NPDR, $P < 0.001$. Tukey HSD post hoc test for ONL-total: control versus NDR, $P = 0.7$; control versus NPDR, $P < 0.001$; NDR versus NPDR, $P < 0.001$.

*Pearson chi-square test.

†One-way analysis of variance test.

‡One-way analysis of variance test and Tukey HSD post hoc test.

foveal HFL area was also lower in the severe group than in the mild group ($P = 0.03$). The moderate and severe NPDR groups had lower total HFL area and thickness than the mild group (all $P < 0.05$). Parafoveal and foveal ONL areas were significantly thicker in the severe NPDR group than in the mild group (all $P < 0.05$). The thicknesses and areas of foveal, parafoveal, and total ONL were higher in the severe group than in the mild group (all $P < 0.05$). There were no significant differences between the mild and moderate groups regarding thicknesses and areas of ONL (Tables 3 and 4). Mean foveal and total c-ONL thicknesses did not differ between the NPDR groups. Thicker parafoveal mean c-ONL was found in the severe NPDR group compared with both the mild and the moderate NPDR groups ($P = 0.01$; Table 4).

Intraclass correlation coefficient and coefficient of variation values indicated excellent intervisit, intraobserver, and interobserver reproducibility of total thickness and area measurements of HFL, OPL, and ONL (Table 5).

Discussion

In this study, we modified the directional OCT strategy of Lujan et al[8,9] and obtained HFL thickness measurements using only the Spectralis OCT software. In addition, the boundaries of the HFL area were determined with the Spectralis OCT software, and only the area was calculated with ImageJ-Fiji software. Using this strategy, we reported a decrease in foveal HFL area and thickness in eyes with NDR compared with healthy eyes. We also detected a decrease in HFL in eyes with NPDR compared with eyes with NDR and healthy eyes. In addition, our study revealed that the HFL is thinner in eyes with severe DR than in eyes with mild DR. As we mentioned before, HFL is composed of Z-shaped Müller cells and photoreceptor axons. It has been previously stated that the retinal neuronal and glial changes caused by DM may precede clinically observed microvascular changes, and accordingly, abnormalities in the multifocal ERG, contrast sensitivity, and microperimetry can be detected in patients with DM without DRP.[15–20] Müller cells are the principal glial cell of the human retina. They span the entire thickness of the retina to provide structural and functional support to retinal neurons.[6,21] Müller cell loss occurs through pyroptosis in DR.[21] During pyroptosis, the nuclei of Müller cells become hypertrophic and cause INL thickening.[2,3,21] However, the number of Müller cells is markedly reduced during this process.[21,22] The reduced number of Müller cells and their outer processes may cause HFL thinning. Although Müller cells' nuclei are oriented radially in the INL, the outer processes of Müller cells are oriented horizontally in the HFL. The association between the thickness of a retinal layer and the number of cells in this layer may be higher in the horizontal orientation of cells.

Table 2. Comparisons of Thickness Measurements Between NDR, NPDR, and Control Groups

	Control (n = 58)	NDR (n = 79)	NPDR (n = 68)	*P*
Central macular thickness (μm)	261.9 ± 21.4	262.9 ± 21.1	267.1 ± 19.7	0.3*
OPL thickness parafovea (μm)	21.8 ± 2.4	22.1 ± 2.9	22.6 ± 2.8	0.3*
OPL thickness fovea (μm)	13.6 ± 3.2	12.4 ± 2.9	12.7 ± 2.6	0.06*
OPL thickness total (μm)	18.7 ± 2.6	18.5 ± 2.4	18.9 ± 2.2	0.5*
HFL thickness parafovea (μm)	42.6 ± 4.6	43.1 ± 7.4	40.6 ± 5.7	0.04†
HFL thickness fovea (μm)	35.9 ± 5.6	33 ± 5.65	29.3 ± 5.2	<0.001†
HFL thickness total (μm)	40.1 ± 4	39.4 ± 4.4	36.4 ± 4.5	<0.001†
ONL thickness parafovea (μm)	37.3 ± 4.3	37.9 ± 5.2	41.6 ± 7.2	<0.001†
ONL thickness fovea (μm)	69.7 ± 10	71.7 ± 10.5	78.2 ± 11.6	<0.001†
ONL thickness total (μm)	49.4 ± 5.8	50.6 ± 6.3	55.3 ± 8.1	<0.001†
c-ONL thickness parafovea (μm)	79.7 ± 7.6	81.1 ± 9.1	82.0 ± 9.22	0.3*
c-ONL thickness fovea (μm)	105.2 ± 10.2	104.1 ± 9.2	107.2 ± 11.4	0.2*
c-ONL thickness total (μm)	92.4 ± 8.2	92.5 ± 8.1	94.6 ± 9.4	0.2*

Tukey HSD post hoc test for HFL-parafovea: control versus NDR, $P = 0.9$; control versus NPDR, $P = 0.04$; NDR versus NPDR, $P = 0.03$. Tukey HSD post hoc test for HFL-fovea: control versus NDR, $P = 0.007$; control versus NPDR, $P < 0.001$; NDR versus NPDR, $P < 0.001$. Tukey HSD post hoc test for HFL-total: control versus NDR, $P = 0.6$; control versus NPDR, $P < 0.001$; NDR versus NPDR, $P = 0.001$. Tukey HSD post hoc test for ONL-parafovea: control versus NDR, $P = 0.7$; control versus NPDR, $P < 0.001$; NDR versus NPDR, $P = 0.001$. Tukey HSD post hoc test for ONL-fovea: control versus NDR, $P = 0.5$; control versus NPDR, $P < 0.001$; NDR versus NPDR, $P = 0.001$. Tukey HSD post hoc test for ONL-total: control versus NDR, $P = 0.6$; control versus NPDR, $P < 0.001$; NDR versus NPDR, $P < 0.001$.

*One-way analysis of variance test.

†One-way analysis of variance test and Tukey HSD post hoc test.

Previous histopathological and OCT studies revealed that cystoid edema in eyes with DR originates from HFL, which is composed of Müller cells and photoreceptor axons.[5,10] In this study, the exclusion of eyes with diabetic macular edema allowed us to evaluate nonedematous HFL with OCT. In addition to significant HFL thinning in patients with DM, we observed localized hyperreflective alterations in the hyporeflective side of the HFL in eyes with NPDR. However, there was no hyperreflective or hyporeflective HFL alteration in this hyperreflective area when the OCT beam was decentered in the opposite direction. Unlike hard exudates, none of these areas had shadowing artifact underneath. Moreover, the finding of localized hyperreflective HFL alterations was more prominent in the severe DR group. Because of the

Table 3. Comparisons of Demographic, Systemic, and Ocular Data and Area Measurements Between Mild NPDR, Moderate NPDR, and Severe NPDR Groups

	Mild NPDR (n = 32)	Moderate NPDR (n = 23)	Severe NPDR (n = 13)	*P*
Sex (male %)	34.4	52.2	61.5	0.2*
Age (years)	57.1 ± 7.8	59 ± 6.5	57.7 ± 7.2	0.6†
Duration of diabetes (years)	13.5 ± 4.2	15.8 ± 4.9	14.1 ± 5.6	0.2†
HbA1c (%)	8 ± 1.1	8.2 ± 1.7	7.9 ± 1.5	0.8†
Refractive error (diopter)	1.1 ± 1	1 ± 0.8	1.4 ± 1.0	0.4†
Axial length (mm)	22.44 ± 0.8	22.5 ± 0.7	22.42 ± 0.9	0.4†
OPL area parafovea (μm^2)	37,217.3 ± 5,092.5	35,275 ± 5,071.8	34,007 ± 5,633	0.3†
OPL area fovea (μm^2)	9,053.4 ± 2,400.3	8,925.6 ± 2,249.3	9,846.6 ± 1,938.8	0.4†
OPL area total (μm^2)	46,270.7 ± 6,508.4	44,200.6 ± 6,315.3	43,853.6 ± 7,013.4	0.6†
HFL area parafovea (μm^2)	74,762.8 ± 8,655	68,772 ± 10,230.2	70,316.9 ± 9,764.8	0.1†
HFL area fovea (μm^2)	22,649.3 ± 5,300.6	20,316.4 ± 4,292.9	17,404.6 ± 5,775.8	0.03‡
HFL area total (μm^2)	97,412.1 ± 10,028.7	89,088.4 ± 12,781.4	87,721.5 ± 10,796.6	0.006‡
ONL area parafovea (μm^2)	69,273.1 ± 10,671.2	70,565.5 ± 10,736	81,674.6 ± 14,267.9	0.02‡
ONL area fovea (μm^2)	65,776.8 ± 9,183.4	69,163.5 ± 11,219.7	76,978.3 ± 11,390	0.04‡
ONL area total (μm^2)	135,049.9 ± 18,430.8	139,729 ± 18,647.9	158,652 ± 23,310.3	0.006‡

Post hoc test for HFL-fovea: mild versus moderate, $P = 0.4$; mild versus severe, $P = 0.03$; moderate versus severe, $P = 0.6$. Post hoc test for HFL-total: mild versus moderate, $P = 0.02$; mild versus severe, $P = 0.03$; moderate versus severe, $P = 1.0$. Post hoc test for ONL-parafovea: mild versus moderate, $P = 1.0$; mild versus severe, $P = 0.02$; moderate versus severe, $P = 0.08$. Post hoc test for ONL-fovea: mild versus moderate, $P = 0.8$; mild versus severe, $P = 0.04$; moderate versus severe, $P = 0.5$. Post hoc test for ONL-total: mild versus moderate, $P = 1.0$; mild versus severe, $P = 0.005$; moderate versus severe, $P = 0.06$.

*Pearson chi-square test.

†Kruskal–Wallis test.

‡Kruskal–Wallis test and post hoc analyses.

Table 4. Comparisons of Thickness Measurements Between Mild NPDR, Moderate NPDR, and Severe NPDR Groups

	Mild NPDR (n = 32)	Moderate NPDR (n = 23)	Severe NPDR (n = 13)	*P*
Central macular thickness (μm)	264.5 ± 15.9	267.4 ± 22.5	273.2 ± 23.1	0.7
OPL thickness parafovea (μm)	23.2 ± 2.6	21.9 ± 3.1	22.3 ± 2.5	0.2*
OPL thickness fovea (μm)	12.6 ± 2.6	12.4 ± 2.8	13.4 ± 2.6	0.5*
OPL thickness total (μm)	19.3 ± 2.2	18.3 ± 2.4	18.9 ± 1.9	0.3*
HFL thickness parafovea (μm)	42.4 ± 5.1	38.7 ± 6.1	39.5 ± 5.8	0.05*
HFL thickness fovea (μm)	31.3 ± 4.6	29.1 ± 4.4	24.7 ± 4.9	<0.001†
HFL thickness total (μm)	38.2 ± 3.7	35.1 ± 4.9	34 ± 3.8	0.003†
ONL thickness parafovea (μm)	40.3 ± 4.5	39.5 ± 6.7	48.6 ± 9.2	<0.001†
ONL thickness fovea (μm)	74.9 ± 8.9	77 ± 11.9	88.5 ± 12.1	0.001†
ONL thickness total (μm)	53.3 ± 5.6	53.5 ± 7.6	63.6 ± 93	<0.001†
c-ONL thickness parafovea (μm)	81.7 ± 7.7	78.8 ± 10.2	88.7 ± 7.93	0.01†
c-ONL thickness fovea (μm)	105.9 ± 9.2	105.6 ± 12.9	112.8 ± 12.6	0.3*
c-ONL thickness total (μm)	93.8 ± 7.5	92.2 ± 10.8	100.8 ± 9.7	0.07*

*Kruskal–Wallis test.

†Kruskal–Wallis test and post hoc analyses.

Post hoc test for HFL-fovea: mild versus moderate, $P = 0.2$; mild versus severe, $P = 0.02$; moderate versus severe, $P = 0.04$. Post hoc test for HFL-total: mild versus moderate, $P = 0.04$; mild versus severe, $P = 0.007$; moderate versus severe, $P = 0.9$. Post hoc test for ONL-parafovea: mild versus moderate, $P = 1.0$; mild versus severe, $P = 0.02$; moderate versus severe, $P = 0.02$. Post hoc test for ONL-fovea: mild versus moderate, $P = 0.9$; mild versus severe, $P = 0.006$; moderate versus severe, $P = 0.03$. Post hoc test for ONL-total: mild versus moderate, $P = 1.0$; mild versus severe, $P = 0.005$; moderate versus severe, $P = 0.01$. Post hoc test for c-ONL-fovea: mild versus moderate, $P = 1.0$; mild versus severe, $P = 0.04$; moderate versus severe, $P = 0.01$.

cross-sectional design of this study and the exclusion of eyes with macular edema, the clinical significance of this OCT finding could not be clearly explained.

In this study, using a modified directional OCT strategy, we reported an increase in ONL (HFL removed) thickness and area in eyes with NPDR compared with eyes with NDR and healthy eyes. However, we found that there is no significant difference between these groups in ONL thickness if HFL was not removed from ONL. Also, the HFL removed ONL is thicker in eyes with severe DR than in eyes with mild DR and moderate DR. However, we detected ONL thickening only at the parafoveal region if HFL was not removed from ONL. There are also conflicting reports in the literature about ONL thickness in early DM and DR. Chen et al[23] investigated retinal layer thicknesses in patients with Type 1 DM (T1DM) and Type 2 DM (T2DM) without DR. They reported thinning of the ONL in T1DM and thickening in T2DM. Ishibashi et al[24] detected a decrease in ONL thickness in patients with T2DM without DR. Orduna-Hospital et al[25] found no differences in ONL thickness between patients with T1DM without DR and healthy control subjects. Vujosevic and Midena[2] reported that there was no difference in ONL thickness between patients with diabetes with and without DR and control subjects. However, none of the previous reports used directional OCT, which provides accurate ONL thickness measurement by separating the HFL.[8] Histologic evaluation of Zucker diabetic fatty rats revealed ONL thickening in the lower half of the retina, probably because of intracellular edema.[26] Eyes with diabetic macular edema were not included in our study, and central macular thickness did not differ between any groups. For these reasons, we thought that ONL thickening in eyes with DR might indicate intracellular edema.

This study has several limitations. First, although the number of participants in the main groups was sufficient, the number of patients in subgroups of NPDR was relatively low. In addition, the cross-sectional design of the study limited our debate on some findings. Especially, there was no clear evidence about the DR-related findings caused by hyperreflective HFL change, and its clinical significance was not fully understood. Although the presence of macular edema was evaluated with the raster scanning

Table 5. Intervisit, Intraobserver, and Interobserver Agreements

	Intervisit		Intraobserver		Interobserver	
	ICC	CV (%)	ICC	CV (%)	ICC	CV (%)
OPL area	0.92	3.64	0.99	0.67	0.99	0.91
OPL thickness	0.90	3.67	0.98	0.94	0.98	1.12
HFL area	0.98	0.94	0.99	0.27	0.99	0.33
HFL thickness	0.96	1.79	0.99	0.17	0.99	0.27
ONL area	0.98	1.36	0.99	0.39	0.99	0.45
ONL thickness	0.92	2.25	0.99	0.68	0.98	0.80

CV, coefficient of variation; ICC, intraclass correlation coefficient.

protocol, HFL measurements performed using a single, horizontal, cross-sectional SD-OCT scan was another limitation of this study.

In conclusion, directional OCT provides isolated thickness and area measurement of HFL. In patients with diabetes, the HFL is thinner, and HFL thinning begins before the presence of DR. Further histopathological studies are needed to clarify changes of HFL before the formation of cystoid edema in eyes with DR. In addition, longitudinal OCT studies may be helpful in demonstrating the clinical significance of hyperreflective HFL alteration.

Key words: diabetic retinopathy, directional optical coherence tomography, Henle fiber layer, outer nuclear layer, outer plexiform layer.

References

1. Cheung N, Mitchell P, Wong TY. Diabetic retinopathy. Lancet 2010;376:124–136.
2. Vujosevic S, Midena E. Retinal layers changes in human preclinical and early clinical diabetic retinopathy support early retinal neuronal and Müller cells alterations. J Diabetes Res 2013;2013:1–8.
3. Yamada Y, Himeno T, Tsuboi K, et al. Alterations of retinal thickness measured by optical coherence tomography correlate with neurophysiological measures in diabetic polyneuropathy. J Diabetes Investig 2021;12:1430–1441.
4. Choi M, Yun C, Oh JH, Kim SW. Foveal Müller cell cone as a prognostic optical coherence tomography biomarker for initial response to antivascular endothelial growth factor treatment in cystoid diabetic macular edema. Retina 2022;42:129–137.
5. Daruich A, Matet A, Moulin A, et al. Mechanisms of macular edema: beyond the surface. Prog Retin Eye Res 2018;63:20–68.
6. Bringmann A, Pannicke T, Grosche J, et al. Müller cells in the healthy and diseased retina. Prog Retin Eye Res 2006;25:397–424.
7. Ramtohul P, Cabral D, Sadda S, et al. The OCT angular sign of Henle fiber layer (HFL) hyperreflectivity (ASHH) and the pathoanatomy of the HFL in macular disease. Prog Retin Eye Res 2022:101135.
8. Lujan BJ, Roorda A, Croskrey JA, et al. Directional optical coherence tomography provides accurate outer nuclear layer and HENLE fiber layer measurements. Retina 2015;35:1511–1520.
9. Lujan BJ, Roorda A, Knighton RW, Carroll J. Revealing Henle's fiber layer using spectral domain optical coherence tomography. Invest Ophthalmol Vis Sci 2011;52:1486–1492.
10. Byeon SH, Chu YK, Hong YT, et al. New insights into the pathoanatomy of diabetic macular edema: angiographic patterns and optical coherence tomography. Retina 2012;32:1087–1099.
11. Wilkinson CP, Ferris FL III, Klein RE, et al. Proposed international clinical diabetic retinopathy and diabetic macular edema disease severity scales. Ophthalmology 2003;110:1677–1682.
12. Delori F, Greenberg JP, Woods RL, et al. Quantitative measurements of autofluorescence with the scanning laser ophthalmoscope. Invest Ophthalmol Vis Sci 2011;52:9379–9390.
13. Ctori I, Gruppetta S, Huntjens B. The effects of ocular magnification on spectralis spectral domain optical coherence tomography scan length. Graefes Arch Clin Exp Ophthalmol 2015;253:733–738.
14. Ersoz MG, Kesim C, Karslioglu MZ, et al. Repeatability of Choroidal Vascularity Index measurements using directional optical coherence tomography images. Retina 2021;41:1723–1729.
15. Yang S, Zhang J, Chen L. The cells involved in the pathological process of diabetic retinopathy. Biomed Pharmacother 2020;132:110818.
16. Alder VA, Su EN, Yu DY, et al. Diabetic retinopathy: early functional changes. Clin Exp Pharmacol Physiol 1997;24:785–788.
17. Han Y, Adams AJ, Bearse MA Jr, Schneck ME. Multifocal electroretinogram and short-wavelength automated perimetry measures in diabetic eyes with little or no retinopathy. Arch Ophthalmol 2004;122:1809–1815.
18. Della Sala S, Bertoni G, Somazzi L, et al. Impaired contrast sensitivity in diabetic patients with and without retinopathy: a new technique for rapid assessment. Br J Ophthalmol 1985;69:136–142.
19. Prager TC, Garcia CA, Mincher CA, et al. The pattern electroretinogram in diabetes. Am J Ophthalmol 1990;109:279–284.
20. Verma A, Rani PK, Raman R, et al. Is neuronal dysfunction an early sign of diabetic retinopathy? Microperimetry and Spectral Domain Optical Coherence Tomography (SD-OCT) Study in individuals with diabetes, but no diabetic retinopathy. Eye 2009;23:1824–1830.
21. Coughlin BA, Feenstra DJ, Mohr S. Müller cells and diabetic retinopathy. Vis Res 2017;139:93–100.
22. Feenstra DJ, Yego EC, Mohr S. Modes of retinal cell Death in diabetic retinopathy. J Clin Exp Ophthalmol 2013;4:298.
23. Chen Y, Li J, Yan Y, Shen X. Diabetic macular morphology changes may occur in the early stage of diabetes. BMC Ophthalmol 2016;16:12.
24. Ishibashi F, Kosaka A, Tavakoli M. The impact of glycemic control on retinal photoreceptor layers and retinal pigment epithelium in patients with type 2 diabetes without diabetic retinopathy: a follow-up study. Front Endocrinol (Lausanne) 2021;12:614161.
25. Orduna-Hospital E, Sanchez-Cano A, Perdices L, et al. Changes in retinal layers in type 1 diabetes mellitus without retinopathy measured by spectral domain and swept source OCTs. Sci Rep 2021;11:10427.
26. Szabó K, Enzsoly A, Dekany B, et al. Histological evaluation of diabetic neurodegeneration in the retina of zucker diabetic fatty (ZDF) rats. Sci Rep 2017;7:8891.